16th World Congress in Computational Mechanics (WCCM)
21-26 July 2024, Vancouver, Canada
A. Korobenko, M. Laforest, S. Prudhomme, R. Vaziri (Eds)

AN ENHANCED FULLY-ADAPTIVE EXPLICIT-IMPLICIT TIME-MARCHING FORMULATION FOR ELASTODYNAMICS

DELFIM SOARES JR.[1], LUCAS R. PINTO[2], ISABELLE S. SOUZA[2] AND WEBE J. MANSUR[2]

[1]Structural Engineering Department, Federal University of Juiz de Fora
CEP 36036-330, Juiz de Fora, MG, Brazil
delfim.soares@ufjf.edu.br

[2]COPPE/Federal University of Rio de Janeiro
CEP 21941-611, Rio de Janeiro, Brazil
lucas.ruffo@engenharia.ufjf.br

Key words: time integration; hybrid analysis; adaptive parameters; elastodynamics.

Abstract. *In this work, an explicit-implicit time-marching formulation, which adapts to the model's properties, its adopted spatial and temporal discretizations, and its computed responses, is studied for elastodynamic analyses. Explicit-implicit approaches have become referred to as effective time-domain solution methodologies since they allow to combine the advantageous features of both explicit and implicit formulations, such as reduced solver efforts and guaranteed stability, providing very attractive techniques. The here discussed time-domain hybrid solution procedure is based on three simple single-step recurrence relationships, which are formulated considering three locally-defined time-integration parameters, namely* α_0^e, α_1^e *and* α_2^e, *and each one of these time-integration parameters is adaptively determined for each element "e" of the adopted spatial discretization. In this context, the* α_0^e *parameter distinguishes explicit (*$\alpha_0^e = 0$*) and implicit (*$\alpha_0^e \neq 0$*) elements, while* α_1^e *and* α_2^e *delineate non-dissipative (*$\alpha_1^e = \alpha_2^e = 0$*) and dissipative (*$\alpha_1^e \neq 0$ *and* $\alpha_2^e \neq 0$*) elements. The adopted non-null expression for* α_0^e *ensures that, in the absence of numerical dissipation, the critical sampling frequency of the method aligns with the maximum sampling frequency of the element, allowing the element to operate as if provided with its critical time-step value. This configuration not only ensures stability, but also better counterbalances the errors of the considered temporal and spatial discretization procedures, enhancing the overall accuracy of the computed discrete solution. On the other hand, the non-null expressions that are defined for* α_1^e *and* α_2^e *are designed to set the bifurcation sampling frequency of the method equal to the maximum sampling frequency of the element and its bifurcation spectral radius to zero. This configuration maximizes numerical dissipation for the element's maximum sampling frequency, effectively dissipating spatially unresolved high-frequency modes while accurately evaluating important low-frequency modes, since the developed adaptive formulation ensures that dissipative elements are activated only when and where it is necessary in the analysis. In addition, an optimal time-step value for maximal computational efficiency is also computed in the proposed solution methodology, based on the "particle swarm optimization" algorithm, which minimizes the expected total number of operations in the hybrid solution process. In this case, the optimal time-step value is determined so that the most efficient distribution of explicit*

and implicit elements is considered in the analysis, providing a highly effective, fully-adaptive and entirely automated, time-domain solution procedure. At the end of this work, numerical results are presented and compared to those of standard time-marching procedures, demonstrating the excellent performance of the reported adaptive hybrid approach.

1 INTRODUCTION

Governing equations for wave propagation problems, as well as many other physical models, necessitate both temporal and spatial discretization techniques for accurate numerical treatment. Typically, these procedures are applied independently. In this scenario, spatial discretization methods, such as the finite element method, are usually first employed to address these governing equations, resulting in a time-domain semi-discrete system of equations. This semi-discrete system is then integrated using a time-marching formulation, which specifies the temporal discretization procedure, enabling the numerical computation of its solution.

The combined performance of the spatial and temporal discretization procedures determines the accuracy and convergence rate of the proposed solution technique. This joint performance is challenging to generically establish, and the labelled convergence rate of many time-marching procedures may lack real significance within this broader context. Although analysing the combined behaviour of temporal and spatial discretization techniques is complex and often impractical (as well as highly specific to particular configurations), these aspects suggest a promising path to enhanced performance when developing time-marching procedures for wave propagation analyses.

Time-marching procedures can generally be categorized into two main families: explicit and implicit methods [1]. Numerous explicit and implicit formulations for time-domain analyses have been frequently reported in the literature. Additionally, in recent years, several composite techniques have been introduced, incorporating both explicit and implicit methodologies. Explicit procedures are typically preferred due to their lower computational costs; however, their use is limited by stability constraints. Conversely, implicit procedures can achieve unconditional stability but require greater computational effort per time step, as a solver routine must be employed to handle the resulting systems of equations associated with these approaches.

In this context, this work reports on a mixed explicit-implicit time-marching formulation proposed by Soares [2], examining its computed responses for elastodynamic analyses. This approach offers a generic conditionally stable time-marching procedure that operates largely at its critical stability limit, regardless of the provided time-step value, ensuring guaranteed stability and leading to enhanced accuracy. Furthermore, explicit or implicit subdomains can be easily defined along the discretized model based on local properties, without significant modifications to the proposed solution procedure.

Historically, the motivation for using combined explicit/implicit time-integration techniques arose partly from issues where meshes contained both relatively flexible and stiff subdomains. In such cases, highly refined subdomains or spatially varying properties within the mesh could necessitate an excessively small time-step value for the entire model, which is particularly constraining for explicit approaches. Over the past decades, improved techniques have been developed to handle the distinction between explicit and implicit subdomains more effectively, and to apply combined formulations more efficiently. However, these coupled approaches

typically require significant input from the user, such as specifications of subdomains/interfaces within the model.

The here reported mixed explicit-implicit time-marching formulation does not involve coupling different time-integration approaches or time-step values, nor does it require interface conditions or extensive information from the user. Instead, it employs a single time-marching framework and one time-step value. This mixed explicit-implicit formulation combines the best features of both standard implicit and explicit approaches in a highly effective and straightforward manner. It incorporates three time-integration parameters, α_0^e, α_1^e and α_2^e, assigned to each element "*e*" of the chosen spatial discretization, offering a highly adaptable and self-adjusting approach. The computation of the α_0^e parameter ensures stability and enhances the accuracy of the analysis, delineating the implicit and explicit elements within the model. Meanwhile, the α_1^e and α_2^e parameters, redefined at each time step, determine non-dissipative and dissipative elements in an efficient numerical dissipative strategy aimed at mitigating the effects of spurious non-physical modes and minimizing undesirable numerical damping errors.

The present work is structured as follows: initially, the governing equations of the model and the adaptive time-integration approach are outlined, detailing the computation of the locally defined self-adjusting time-integration parameters. Subsequently, numerical applications are provided to showcase the good accuracy and efficacy of the reported procedure. Finally, conclusions are drawn, summarizing the numerous positive attributes of the novel methodology.

2 GOVERNING EQUATIONS AND TIME INTEGRATION STRATEGY

The semi-discrete system of equations describing a elastodynamic model may be written as:

$$\mathbf{M}\ddot{\mathbf{U}}(t) + \mathbf{C}\dot{\mathbf{U}}(t) + \mathbf{K}\mathbf{U}(t) = \mathbf{F}(t) \tag{1}$$

where the symbols $\mathbf{M}$, $\mathbf{C}$, and $\mathbf{K}$ denote the mass, damping, and stiffness matrices of the problem, respectively. The force vector is represented by $\mathbf{F}(t)$, while $\mathbf{U}(t)$, $\dot{\mathbf{U}}(t)$ and $\ddot{\mathbf{U}}(t)$ correspond to the displacement, velocity and acceleration vectors, respectively. The initial conditions of the model are defined as $\mathbf{U}^0 = \mathbf{U}(0)$ and $\dot{\mathbf{U}}^0 = \dot{\mathbf{U}}(0)$, where $\mathbf{U}^0$ and $\dot{\mathbf{U}}^0$ refer to the initial displacement and velocity vectors, respectively.

By integrating Eq. (1) over time, considering a time-domain discretization defined by $t^{n+1} = t^n + \Delta t$, where Δt represents the adopted time-step, one may write:

$$\mathbf{M}\int_{t^n}^{t^{n+1}} \ddot{\mathbf{U}}(t)dt + \mathbf{C}\int_{t^n}^{t^{n+1}} \dot{\mathbf{U}}(t)dt + \mathbf{K}\int_{t^n}^{t^{n+1}} \mathbf{U}(t)dt = \int_{t^n}^{t^{n+1}} \mathbf{F}(t)dt \tag{2}$$

where the integrals on the left-hand side of Eq. (2) can be defined as:

$$\int_{t^n}^{t^{n+1}} \ddot{\mathbf{U}}(t)dt = \dot{\mathbf{U}}^{n+1} - \dot{\mathbf{U}}^n \tag{3a}$$

$$\int_{t^n}^{t^{n+1}} \dot{\mathbf{U}}(t)dt = \mathbf{U}^{n+1} - \mathbf{U}^n \tag{3b}$$

$$\int_{t^n}^{t^{n+1}} \mathbf{U}(t)dt = \Delta t\mathbf{U}^n + \frac{1}{2}(1-\alpha_0\,)\Delta t^2\dot{\mathbf{U}}^n + \frac{1}{2}\alpha_0\,\Delta t^2\dot{\mathbf{U}}^{n+1} \tag{3c}$$

The integral on its right-hand side, representing the time integral of the force term, may be denoted as $\bar{\mathbf{F}}$. This integral can be computed analytically or using any standard numerical procedure for calculating the numerical value of a definite integral. In Eqs. (3a–c), $\mathbf{U}^{n+1}$ and $\dot{\mathbf{U}}^{n+1}$ represent approximations for $\mathbf{U}(t^{n+1})$ and $\dot{\mathbf{U}}(t^{n+1})$, respectively, and α_0 denotes a time-integration parameter for the proposed solution procedure. Additionally, $\mathbf{U}^{n+1}$ and $\dot{\mathbf{U}}^{n+1}$ can be related to each other through the following finite difference expression:

$$\mathbf{U}^{n+1} = \mathbf{U}^n + \frac{1}{2}\Delta t\dot{\mathbf{U}}^n + \frac{1}{2}\Delta t\dot{\mathbf{U}}^{n+1} \tag{4}$$

which, when applied together with Eqs. (3a–c) to Eq. (2), yields the following recursive relation:

$$\begin{aligned}\left(\mathbf{M} + \frac{1}{2}\Delta t\mathbf{C} + \frac{1}{2}\alpha_0\,\Delta t^2\mathbf{K}\right)\dot{\mathbf{U}}^{n+1} \\ = \bar{\mathbf{F}} + \mathbf{M}\dot{\mathbf{U}}^n - \frac{1}{2}\Delta t\mathbf{C}\dot{\mathbf{U}}^n - \Delta t\mathbf{K}(\mathbf{U}^n + \frac{1}{2}(1-\alpha_0\,)\Delta t\dot{\mathbf{U}}^n)\end{aligned} \tag{5}$$

In this case, the velocities of the model at the current time step can be computed using Eq. (5), and then Eq. (4) can be employed to assess its displacements. To introduce controllable algorithmic damping into the analysis, the velocity vector of the model, computed as indicated by Eq. (5), can be modified, considering an update of its value as indicated by:

$$\dot{\mathbf{U}}^{n+1} \Leftarrow \dot{\mathbf{U}}^{n+1} - \mathbf{M}^{-1}\mathbf{K}(\frac{1}{2}\alpha_1\,\Delta t^2\dot{\mathbf{U}}^n + \frac{1}{2}\alpha_2\,\Delta t^2\dot{\mathbf{U}}^{n+1}) \tag{6}$$

where α_1 and α_2 represent additional time-integration parameters for the method, which delineate the numerical dissipative features of the technique.

Once Eqs. (4-6) are presented, they can be reformulated and aligned in a sequential order to establish the following time-marching solution algorithm:

$$(\mathbf{M} + \frac{1}{2}\Delta t\mathbf{C} + \alpha'_0\,\mathbf{K})\Delta\dot{\mathbf{U}} = \bar{\mathbf{F}} - \Delta t(\mathbf{C}\dot{\mathbf{U}}^n + \mathbf{K}(\mathbf{U}^n + \frac{1}{2}\Delta t\dot{\mathbf{U}}^n)) \tag{7a}$$

$$\dot{\mathbf{U}}^{n+1} = \dot{\mathbf{U}}^n + \Delta\dot{\mathbf{U}} - \mathbf{M}^{-1}\mathbf{K}(\alpha'_1\,\dot{\mathbf{U}}^n + \alpha'_2\,\dot{\mathbf{U}}^{n+1}) \tag{7b}$$

$$\mathbf{U}^{n+1} = \mathbf{U}^n + \frac{1}{2}\Delta t(\dot{\mathbf{U}}^n + \dot{\mathbf{U}}^{n+1}) \tag{7c}$$

where $\alpha'_i = \frac{1}{2}\Delta t^2\alpha_i$, for i = 0, 1 and 2. As one may observe, Eq. (7a) reproduces Eq. (5), considering $\Delta\dot{\mathbf{U}} = \dot{\mathbf{U}}^{n+1} - \dot{\mathbf{U}}^n$, and Eq. (7b) replicates the updating of the velocity vector, as indicated by Eq. (6), once non-null values are considered for α'_1 and α'_2 .

As previously highlighted, the solution algorithm described by equations (7a-c) are here implemented considering a local approach. In this context, the local time-integration parameters α'^e_0, α'^e_1 and α'^e_2 are computed as functions of the element's maximal sampling frequency Ω_e^{max} (where $\Omega_e^{max} = \omega_e^{max}\Delta t$ and ω_e^{max} represent the highest natural frequency of the element "e", evaluated based on its local matrices $\mathbf{M}_e$ and $\mathbf{K}_e$) and its damping ratio ξ_e (defined as $\xi_e = \varsigma_e(2\rho_e\omega_e^{max})^{-1}$, where ς_e and ρ_e are the physical parameters of the model describing matrices $\mathbf{C}_e$ and $\mathbf{M}_e$, respectively). In this scenario, α'^e_0 is determined based on a stability criterion. Thus,

if Ω_e^{max} is lower than or equal to the stability limit of the method's associated explicit formulation (i.e., if $\Omega_e^{max} \leq \Omega^{lim}$), $\alpha'^e_0 = 0$. In this work, lumped mass and damping matrices are used, resulting in a locally diagonal effective matrix for $\alpha'^e_0 = 0$, which designates an explicit element. Conversely, if $\alpha'^e_0 \neq 0$, the element is designated as implicit. The reported explicit procedure has its stability limit defined by $\Omega^{lim} = 2$, which corresponds to the critical sampling frequency of the Central Difference (CD) method, to which the proposed technique is spectrally equivalent when $\alpha'_0 = \alpha'_1 = \alpha'_2 = 0$. Following this adaptive approach, explicit and implicit elements are automatically assigned along the discretized model.

Similarly to the α'^e_0 parameter, the α'^e_1 and α'^e_2 parameters designate the dissipative ($\alpha'_1 \neq 0$ and $\alpha'_2 \neq 0$) and non-dissipative ($\alpha'_1 = \alpha'_2 = 0$) elements of the model. When $\alpha'^e_1 = \alpha'^e_2 = 0$, the velocity update is given by $\dot{\mathbf{U}}^{n+1} = \dot{\mathbf{U}}^n + \Delta\dot{\mathbf{U}}$, and no numerical dissipation is introduced. This also avoids the computation of the local remaining term of equation (7b), resulting in a solution algorithm with reduced computational effort. However, for other values of the time-integration parameters, algorithmic damping can be employed to eliminate spurious non-physical oscillations arising from the excitation of spatially unresolved high-frequency modes. This allows for the localized application of numerical damping whenever and wherever necessary, enhancing accuracy.

The objective of algorithmic damping is to mitigate spurious non-physical oscillations by introducing high-frequency numerical damping without affecting the important low-frequency modes. This adaptive dissipative procedure can be implemented based on an oscillatory criterion. If the computed response of a degree of freedom oscillates over time, the time-integration parameters of the neighboring elements are adjusted, locally introducing algorithmic damping. By rewriting the velocity update described by Eq.(6) as $\dot{\mathbf{U}}^{n+1} \Leftarrow \dot{\mathbf{U}}^{n+1} - \mathbf{M}^{-1}\mathbf{V}$, in which an auxiliary vector $\mathbf{V}$ is introduced, this strategy can be mathematically defined as follows, for each time step of the analysis: (i) establish an oscillatory parameter ϕ_η for each degree of freedom η, as indicated by: if $\dot{U}_\eta^{n+1}\dot{U}_\eta^n < 0$, $\phi_\eta = 1$; otherwise, $\phi_\eta = 0$; (ii) if $[\sum \phi_\eta]_e > 0$, at least one degree-of-freedom of the element is oscillating, and the local vector $\mathbf{V}_e = \mathbf{K}_e(\alpha'^e_1\dot{\mathbf{U}}_e^n + \alpha'^e_2\dot{\mathbf{U}}_e^{n+1})$ is then computed and assembled into the global vector $\mathbf{V}$, introducing algorithmic damping into the analysis; (iii) if $[\sum \phi_\eta]_e = 0$, the degrees-of-freedom of the element are not oscillating, and $\mathbf{V}_e = \mathbf{0}$ is then defined, introducing no local numerical dissipation into the analysis.

The expressions for the local time-integration parameters, considering both explicit and implicit elements, are provided in Tab. 1. Using these non-null expressions for α'^e_1 and α'^e_2, the bifurcation spectral radius of the method becomes null ($\rho_b = 0$), and its bifurcation sampling frequency equals the maximum sampling frequency of the focused element ($\Omega_b \equiv \Omega_e^{max}$). Consequently, maximal possible numerical damping is provided for Ω_e^{max}, resulting in a highly effective local dissipative procedure. Similarly, the non-null expression provided for α'^e_0 in Tab. 1 (for implicit analysis) is formulated so that when numerical dissipation is not applied, the critical sampling frequency of the method becomes equal to the maximal sampling frequency of the focused element (i.e., $\Omega_c \equiv \Omega_e^{max}$). This design ensures that the errors of the proposed time-marching technique can better counterbalance the errors of equivalent spatial discretization procedures, leading to enhanced accuracy through this combined spatial/temporal formulation.

In the discussed hybrid formulation, an optimal time-step value, which optimizes the amount of explicit and implicit elements in the analysis for computational efficiency, may also be determined. In this context, the "particle swarm optimization" algorithm [3] is here employed to compute an optimal Δt value that minimizes the expected total number of operations in the discussed hybrid solution process, turning it always more efficient than purely explicit or purely implicit solutions.

Table 1: Adaptive parameters ($\alpha'^{e}_{i} = \frac{1}{2}\Delta t^2 \alpha^{e}_{i}$)

Explicit ($\Omega_e^{max} \leq 2$)	$\alpha_0^e = 0$
	$\alpha_1^e = 2(1 - \Omega_e^{max}\xi_e)\Omega_e^{max^{-4}}$
	$\alpha_2^e = 2(\Omega_e^{max^2} - \Omega_e^{max}\xi_e - 1)\Omega_e^{max^{-4}}$
Implicit	$\alpha_0^e = 1/2 - 2\Omega_e^{max^{-2}}$
	$\alpha_1^e = (\Omega_e^{max}/2 - 2\xi_e)\Omega_e^{max^{-3}}$
	$\alpha_2^e = (3\Omega_e^{max}/2 - 2\xi_e)\Omega_e^{max^{-3}}$

3 NUMERICAL EXAMPLES

This section explores two examples. Initially, in the first example, the axial motion of an elastic rod is examined, which is excited by Neumann boundary conditions. In the sequence, two synthetic models with complexities comparable to real geological applications are explored in the second example, demonstrating the effectiveness of the discussed methodology for analyzing large-scale geophysical problems, such as those encountered in the OIL & GAS industry.

The Finite Element Method (FEM) is here employed for the spatial discretization, utilizing linear triangular elements. The responses assessed by the reported solution procedure are compared to those obtained from widely recognized time-marching methodologies, such as the Trapezoidal Rule [4], the Generalized-α method [5] (considering ρ_∞= 0.5), and the Bathe method [6]. Concerning the reported technique, results are additionally presented utilizing two distinct approaches for the first example: (i) an explicit-implicit formulation, where explicit-implicit analyses are conducted, and the expressions from the first and second blocks of Tab. 1 are applied to the elements of the model at which $\Omega_e^{max} \leq 2$ and $\Omega_e^{max} > 2$, respectively; and (ii) a purely implicit formulation, where only implicit analyses are employed, and the second block of expressions from Tab 1 is utilized regardless of the Ω_e^{max} value of the element.

To assess the errors in the computed responses of the first example, and compare the performances of the aforementioned time-marching formulations, Eq. (8) is used, where u denotes the computed field describing the time-history result for a selected degree-of-freedom, u_a represents its analytical counterpart, and N stands for the total number of time steps in the analysis.

$$Error = \left[\sum_{n=1}^{N}(u^n - u_a(t^n))^2 / \sum_{n=1}^{N}(u_a(t^n))^2\right]^{1/2} \tag{8}$$

3.1 Example 1

The first application considers a rectangular solid behaving like a one-dimensional rod, fixed at its left border and subjected to a suddenly applied constant force at its right border. Analytical solutions for the longitudinal displacements of this application are available in [2]. Both a uniform structured and an irregular unstructured FEM mesh with 4000 linear triangular elements are used to spatially discretize the model, and various Δt values are adopted for the analyses. For the regular spatial discretization, just one Ω_e^{max} value arises for the entire domain. For the irregular spatial discretization, on the other hand, several Ω_e^{max} values occur simultaneously, providing a more complex configuration.

The adopted time-step values for this application are: $\Delta t = 5 \cdot 10^{-4} s$, $\Delta t = 7.5 \cdot 10^{-4} s$, $\Delta t = 10^{-3} s$, $\Delta t = 1.25 \cdot 10^{-3} s$, and $\Delta t = 1.5 \cdot 10^{-3} s$. Fig. 1 depicts the FEM meshes and their Ω_e^{max} distributions for $\Delta t = 10^{-3} s$. For this time-step value, $\Omega_e^{max} = 3$ for all the elements of the regular mesh, resulting in a purely implicit solution for this configuration, while $1.6891 \leq \Omega_e^{max} \leq 7.0912$ for the irregular mesh, allowing both explicit and implicit elements to simultaneously occur. Tab. 2 shows the percentages of explicit elements distributed along the model for the adopted five time-step values. As expected, for the irregular spatial discretization, the number of implicit elements increases with larger Δt values to ensure stability. For $\Delta t = 5 \cdot 10^{-4} s$, nearly the entire domain of the model is defined as explicit, with only 9.52% of elements being implicit. In contrast, for $\Delta t = 1.25 \cdot 10^{-3} s$, and $\Delta t = 1.5 \cdot 10^{-3} s$, all elements are implicit.

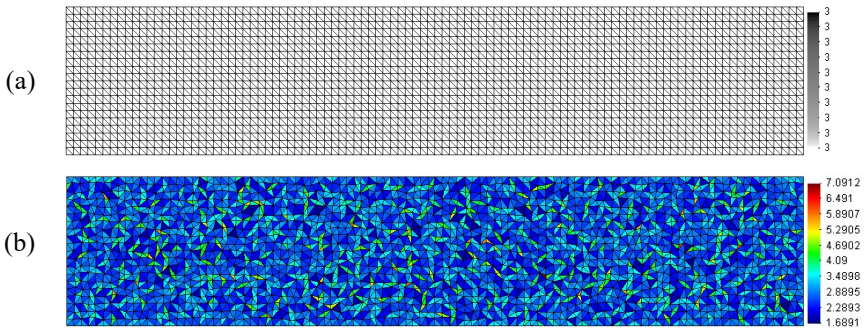

Figure 1: Adopted meshes and Ω_e^{max} distribution along the model (first example), for Δt = 10^{-3} s: (a) regular mesh; (b) irregular mesh.

Table 2: Percentage of explicit elements

Δt (10^{-4}s)	irregular (%)	regular (%)
5	90.48	100
7.5	33.05	0
10	1.85	0
12.5	0	0
15	0	0

Fig. 2 provides relative error results for the axial displacements at the middle of the rod, which are computed considering the referred time-marching techniques and time-step values. As one may observe, the reported novel approach yields significantly more accurate results than standard techniques, even outperforming a composite methodology that uses two solving procedures per time step. Notably, for this application, the purely implicit approach of the

discussed formulation provides more accurate responses than the reported mixed explicit-implicit methodology, highlighting the effectiveness of the proposed adaptive strategy.

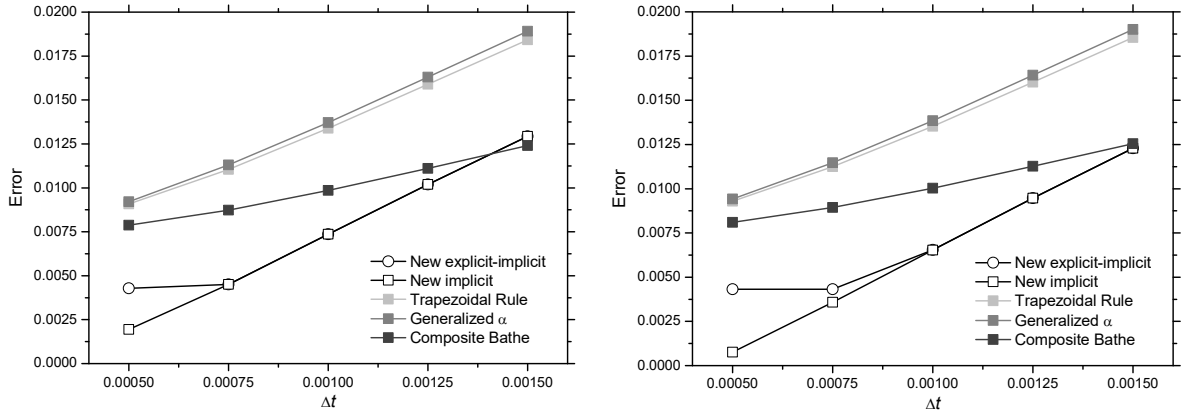

(a) (b)

Figure 2: Error results for the first example: (a) regular mesh; (b) irregular mesh.

Fig. 3 shows time-history results for the axial displacement at the middle of the rod (zoomed view), illustrating the excellent accuracy of the proposed technique. Results are presented for $\Delta t = 5 \cdot 10^{-4} s$ with both regular and irregular FEM meshes. As indicated in this figure, the adaptive methodology effectively quickly eliminates spurious oscillations, unlike standard techniques.

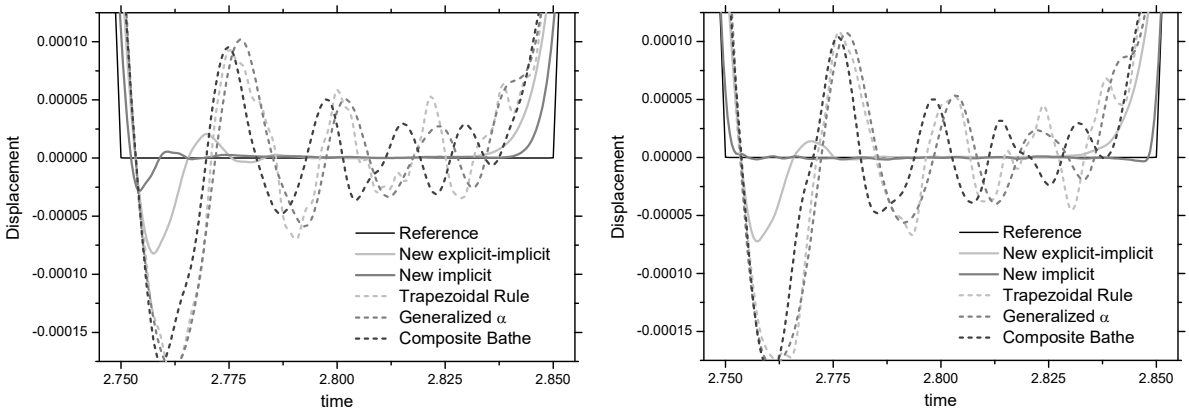

(a) (b)

Figure 3: Zoomed view of the time-history results for the axial displacements at the middle of the rod, for Δt = $5{\cdot}10^{-4}$ s: (a) regular mesh; (b) irregular mesh.

Fig. 4 provides relative error results for the computed velocities, further confirming the superior accuracy of the new formulation, particularly regarding irregular spatial discretizations. Fig. 5 provides snapshots of the $\alpha'^{e}_{1} + \alpha'^{e}_{2}$ values, indicating the dissipative elements along the irregular mesh at t = 1s, t = 2s and t = 3s. This figure highlights that, in the discussed approach, algorithmic dissipation is locally applied only when and where it may be necessary, enhancing the performance of the referred time-marching technique.

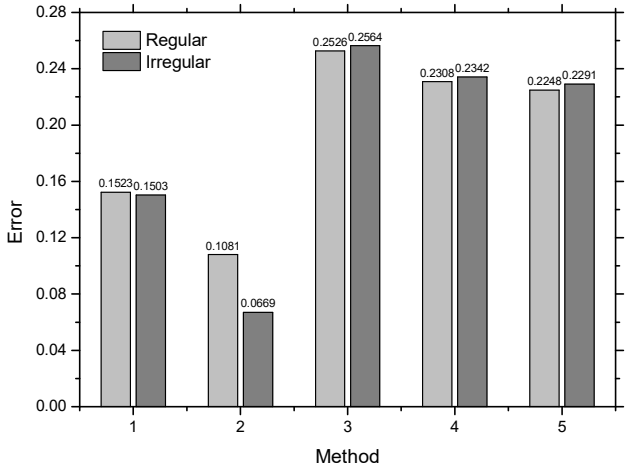

Figure 4 Error results for the computed axial velocities at the middle of the rod, considering $\Delta t = 5 \cdot 10^{-4}$s and regular and irregular meshes: 1 – New explicit-implicit; 2 – New implicit; 3 – Trapezoidal Rule; 4 – Generalized α; 5 – Composite Bathe.

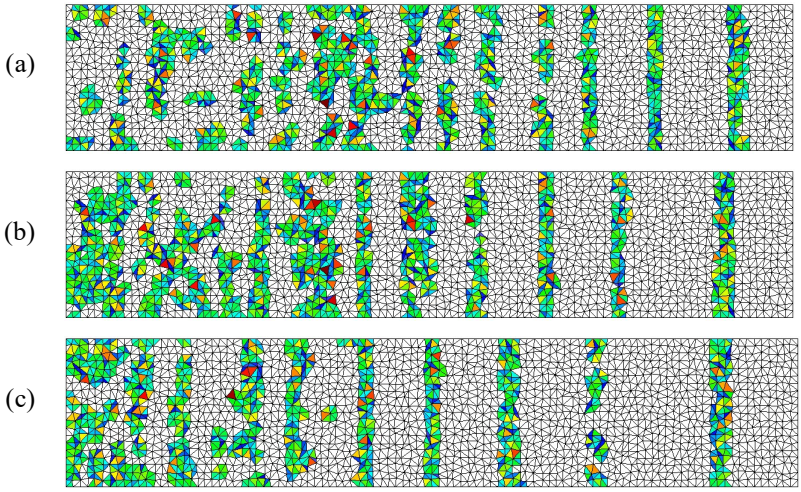

Figure 5: Evolution of the dissipative elements along the explicit-implicit analysis of the first example (dissipative elements are coloured, indicating its $\alpha'^{e}_{1} + \alpha'^{e}_{2}$ value), considering the adopted irregular mesh and $\Delta t = 10^{-3}$s: (a) t = 1s; (b) t = 2s; (c) t = 3s.

3.2 Example 2

In this subsection, two geological subsurface applications are studied to further demonstrate the robustness and efficiency of the discussed hybrid methodology. These synthetic geological models are designed to mimic the complexity of real subsurface structures, making them ideal for evaluating the applicability of the discussed technique in industrial contexts. The first model, commonly referred to as the 2DEW [7] model (see Fig. 6(a)), replicates the salt formations found in the Gulf of Mexico. The second model, known as the 2004 BP model [8] (see Fig. 6(b)), offers a composite representation of various geological sections from different regions, including the western and central/east Gulf of Mexico, as well as elements observed in the Caspian, North, and Trinidad seas. Due to the high computational costs associated with these models, the Bathe method is not here employed for their analyses.

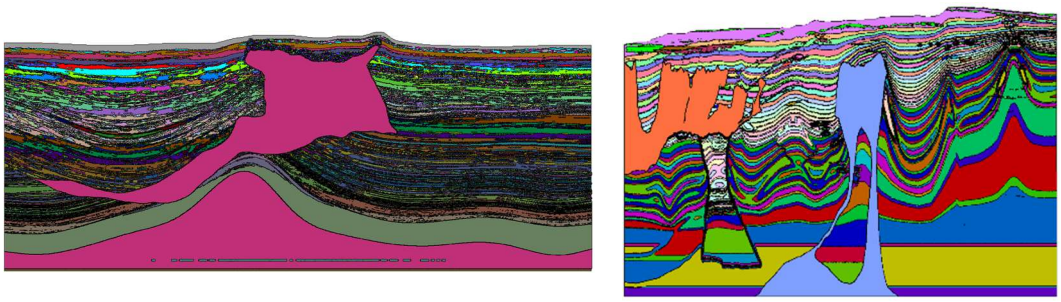

(a) (b)

Figure 6: Geological models: (a) model 1 – 2DEW [7]; and (b) model 2 – 2004 BP [8].

The first model represents an area of 35 km x 15 km, discretized using a mesh of 717,139 linear triangular elements. It is excited by a force applied at its upper surface at x = 17440 m. The second model considers an area of 67.5 km x 46 km, discretized using a mesh of 2,574,204 linear triangular elements, and is excited by a force applied at x = 33750 m. In both applications, perfectly matched layers (PMLs) [9] are employed to avoid wave reflections at the vertical and lower horizontal boundaries of the discretized domain. The thicknesses of these PMLs are 1 km for both models.

Fig. 7 illustrates the computed subdomains for these two models, considering the discussed explicit-implicit methodology and optimal time-step values. In this case, the following subdivisions are obtained, considering the percentages of elements in each subdomain: (i) model 1 – 76.69% explicit and 23.31% implicit, for $\Delta t = 3.4851 \cdot 10^{-3}$ s; and (ii) model 2 – 86.49% explicit and 13.51% implicit, for $\Delta t = 4.1842 \cdot 10^{-3}$ s.

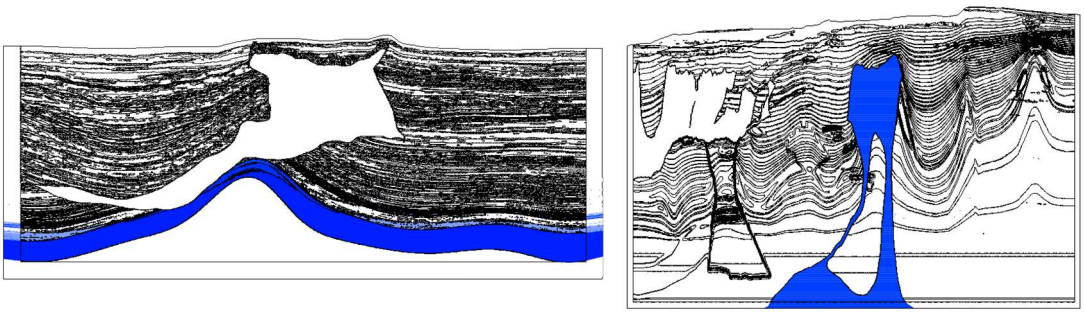

(a) (b)

Figure 7: Computed subdomains for (a) model 1 – 2DEW and (b) model 2 – 2004 BP: explicit subdomains are depicted in white, whereas implicit subdomains are depicted in blue.

In Tab. 3, a detailed description of the performance of each adopted solution technique for each model is provided. The new technique emerges as the most efficient procedure, delivering results more than four to more than seven times faster than the considered standard formulations. Figs. 8 and 9 present screenshots depicting the computed displacement results (in modulus) for models 1 and 2, respectively. As these figures illustrate, the discussed hybrid methodology yields responses comparable to those of the Generalized-α method; however, as indicated in Tab. 3, it does so considering significantly lower CPU times.

Table 3: Performance of the methods for the second example

Model	Method	Parameter evaluation (s)	Pre-solver computation (s)	Time-marching procedure (s)	Total CPU time (s)
1	Trapezoidal Rule	-	456.83 (5.88)	2982.19 (4.22)	3462 (4.32)
	Generalized-α	-	472.62 (6.08)	3248.56 (4.59)	3747 (4.69)
	New explicit-implicit	0.453	77.65 (1.00)	706.69 (1.00)	800 (1.00)
2	Trapezoidal Rule	-	16913.74 (42.83)	200042.42 (6.91)	216990 (7.40)
	Generalized-α	-	17779.33 (45.02)	213944.34 (7.40)	231760 (7.90)
	New explicit-implicit	0.589	394.89 (1.00)	28909.96 (1.00)	29321 (1.00)

*Relative values are provided in parenthesis

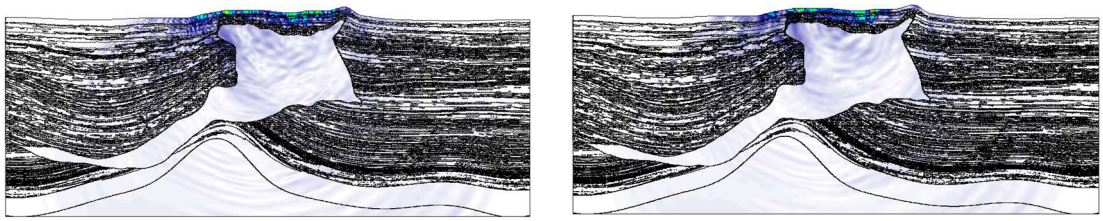

(a) (b)

Figure 8: Computed result along the discretized domain of model 1, at 5s: (a) Generalized-α method; and (b) discussed explicit-implicit approach.

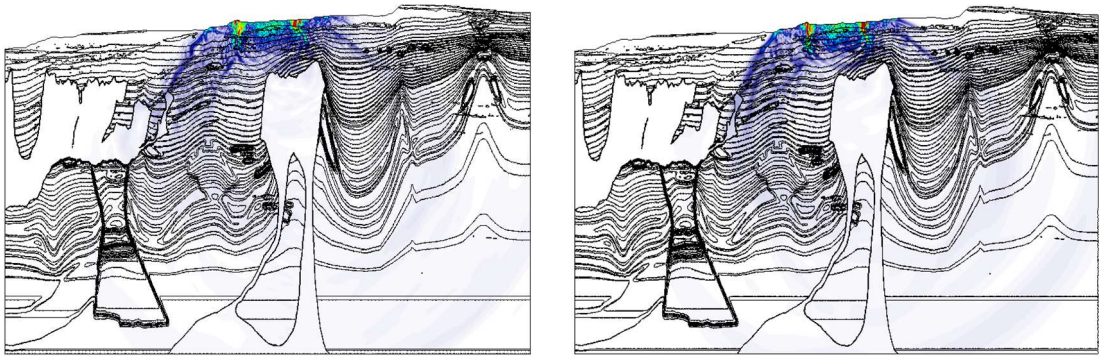

(a) (b)

Figure 9: Computed result along the discretized domain of model 2, at 20s: (a) Generalized-α method; and (b) discussed explicit-implicit approach**.**

4 CONCLUSIONS

This work investigates a mixed self-adjustable explicit-implicit time-marching formulation for analysing wave propagation models. The discussed technique offers guaranteed stability by adding implicit elements into the analysis, as well as it reduces computational efforts by incorporating explicit elements, thus combining the best features of both implicit and explicit formulations. As reported, the technique relies on locally defined time-integration parameters that adaptively adjust themselves based on the characteristics of the discretized model and the evolution of computed responses. In this sense, it may engender enhanced accuracy, as well as effectively dissipate the influence of spurious high-frequency modes without significantly compromising the accuracy of the lower mode contributions. The superior performance of the discussed methodology, in terms of both accuracy and efficiency, is illustrated in the previous

section, at which the novel formulation consistently yields substantially better results than standard approaches.

The main features of the discussed time-marching formulation may be summarized as follows: (i) it stands as a single-step procedure; (ii) it is truly self-starting; (iii) it is locally defined and it self-adjusts to the properties of the discretized model; (iv) it provides a link between the adopted temporal and spatial solution techniques, allowing their errors to be better counterbalanced; (v) it enables stable analyses; (vi) it provides enhanced accuracy; (vii) it engenders advanced controllable algorithmic dissipation in the higher modes, considering optimized adaptive calculations; (viii) it stands as a single-solver framework based on reduced systems of equations; (ix) it enables mixed analyses considering a single group of recurrence relationships, avoiding elaborated coupling procedures and/or interface treatments; (x) it is simple to implement and to apply; (xi) it is entirely automated, requiring no decision nor effort from the user; (xii) it may consider optimal time-step values, further enhancing the efficiency of the analysis. As one can observe, the proposed technique is very attractive, providing the main positive features that are requested from an effective time-marching procedure.

Acknowledgements. *The authors acknowledge the support of the Human Resources Program of Agência Nacional do Petróleo, Gás Natural e Biocombustíveis – PRH-9.1/ANP, maintained with resources from the RD&I Clause of Resolution ANP nº 50/2015, CNPq (Conselho Nacional de Desenvolvimento Científico e Tecnológico), and PETROBRAS (CENPES 21066).*

REFERENCES

[1] Tamma, K. K., Zhou, X., & Sha, D. The time dimension: a theory towards the evolution, classification, characterization and design of computational algorithms for transient/dynamic applications. *Archives of Computational Methods in Engineering*, 7, 67-290 (2000).

[2] Soares Jr, D. "An enhanced explicit–implicit time-marching formulation based on fully-adaptive time-integration parameters." *Computer Methods in Applied Mechanics and Engineering* 403 (2023): 115711.

[3] Kennedy, J., & Eberhart, R. Particle swarm optimization. *In Proceedings of ICNN'95-international conference on neural networks*; Vol. 4, pp. (1995) IEEE.

[4] N.M. Newmark, A method of computation for structural dynamics, *Journal Engineering Mechanics Division,* ASCE 85 (1959) 67–94.

[5] Chung, J., & Hulbert, G. A time integration algorithm for structural dynamics with improved numerical dissipation: the generalized-α method. ASME. *J. Appl. Mech*, (1993) 60(2): 371–375.

[6] Bathe, K. J., & Baig, M. M. I. On a composite implicit time integration procedure for nonlinear dynamics. *Computers & Structures*, (2005) 83(31-32), 2513-2524.

[7] Fehler, M. (2012). SEAM update: SEAM phase I-RPSEA update: Status of simulations. *The Leading Edge*, 31(12), 1424-1426.

[8] Billette, F. J., & Brandsberg-Dahl, S. The 2004 BP velocity benchmark. In 67th EAGE Conference & Exhibition. *European Association of Geoscientists & Engineers*. (2005)

[9] Basu, U. Perfectly matched layers for acoustic and transient waves. *Dam Safety Research Program U.S. Department of the Interior Bureau of Reclamation*. (2008)